The Magnetic Phase Transition and Spin Wave Excitations in the Perovskite $La_{0.7}Sr_{0.3}MnO_3$: An Experiment Using the SPINS Triple-Axis Spectrometer

Summer School on Methods and Applications of Neutron Spectroscopy

NIST Center for Neutron Research

Jae-Ho Chung, William Ratcliff, and Owen Vajk

June 20-23, 2005

Abstract

Using elastic and inelastic neutron scattering with a triple-axis spectrometer, we will study the ferromagnetic transition in a perovskite $La_{0.7}Sr_{0.3}MnO_3$ and its spin wave excitations due to cooperative fluctuations of ordered spins. This experiment will give us an opportunity to learn basic principles of triple-axis spectroscopy, and at the same time will demonstrate that neutron scattering is an excellent probe to study static and dynamic magnetic correlations in condensed matter systems.

Objectives

1. To understand what is measured in a neutron inelastic scattering experiment.
2. To gain a basic understanding of the principles of Triple-Axis Spectroscopy (TAS).
3. To learn how to analyze the TAS data obtained to extract physical information about the system being studied.
4. To observe the ferromagnetic phase transition in the perovskite $La_{0.7}Sr_{0.3}MnO_3$, and study the cooperative fluctuations of the ordered spins.

I. INTRODUCTION

For years, magnetic media have been the basis for storing information in the computer industry. The information is stored in the form of bits which are read by magnetic read heads. These magnetic read heads work by displaying a small change in their electrical resistivity as they pass over a bit. This change in the resistivity under an applied magnetic field is called magnetoresistance (MR) and materials evincing it are called magnetoresistive. The magneoresistance is generally only a few percent in metals and semiconductors. One such material was Permalloy, an alloy of Iron and Nickel. The current read heads in hard drives are giant magnetoresistive (GMR) type based on multilayer thin film technology. Recently, improved material synthesis techniques developed in the quest to develop high temperature superconductors led researchers to revisit the doped $LaMnO_3$ class of materials. In these manganites, the application of a magnetic field causes the resistivity to drop by several orders of magnitude, which would be ideal for device applications. Such materials were said to possess colossal magnetoresistance (CMR) as compared to the much smaller MR or GMR observed before. The basic physics behind this colossal drop of the resistivity in the presence of a magnetic field is an insulator-to-metal transition[1] which results in electronic phase separation (in which two electronic phases are spatially distinct) between a ferromagnetic metallic and a paramagnetic insulating states.

The particular material that we will examine is $La_{0.7}Sr_{0.3}MnO_3$, where doped holes induce ferromagnetism and metallic conductivity. The parent compound, $LaMnO_3$ is an antiferromagnetic insulator. Let us first briefly discuss how doped holes create metallic conductivity.

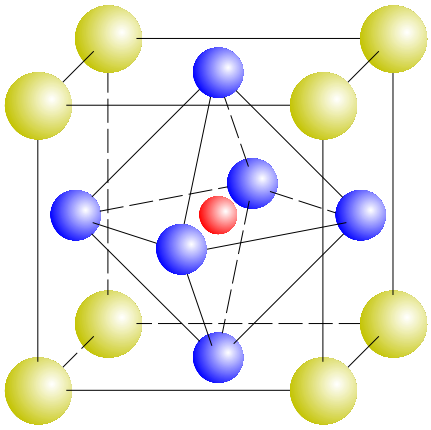

FIG. 1: A unit cell of a cubic pervoskite ABO_3. The small red, medium blue, and large yellow spheres are B, A, and O sites, respectively.

In a crystal, the wave functions of electrons on neighboring atoms mix and their energy levels expand into bands of allowed energies. Because electrons follow the Pauli Exclusion principle, they cannot occupy the same states simultaneously. Thus, the electrons fill the available states up to an energy known as the Fermi energy, E_F. In metals, electrons near E_F are still free to move because there are still available but unoccupied states in the band. An insulator is the case when all the available states are filled with electrons. While generally we think of current as electrons flowing though a solid, current can also be induced if some of the electrons in the occupied states are removed (or in other words *holes* are *doped*), potentially allowing other electrons to hop in. The holes often have similar mobility as electrons and thus can create metallic conductivity.

The manganites typically have crystal structures derived from cubic perovskite lattices (see Fig. 1), in which each Mn cation is surrounded by six oxygen ions which form an octahedron around it. In this environment, the crystal fields of the ligands split the degeneracy of the $3d$-orbitals on the Mn site into three degenerate t_{2g} and two degenerate e_g orbitals. (see Fig. 2(a)). Strong Hund's rule coupling (related to the minimization of Coulomb repulsion of the electrons on a given atom, while satisfying the Pauli exclusion principle) results in the spins of the $3d$ electrons being aligned. As a result, the t_{2g} spins are localized while the e_g spin has an available state to hop. However, the e_g spin makes the Mn^{3+} ion Jahn-Teller (JT) active.[2] That is, the system is able to lower its energy by allowing a distortion of the oxygen environment. This distortion breaks the degeneracy of the e_g orbitals, with one orbital becoming lower in energy and the other higher than in the degenerate case. (also see

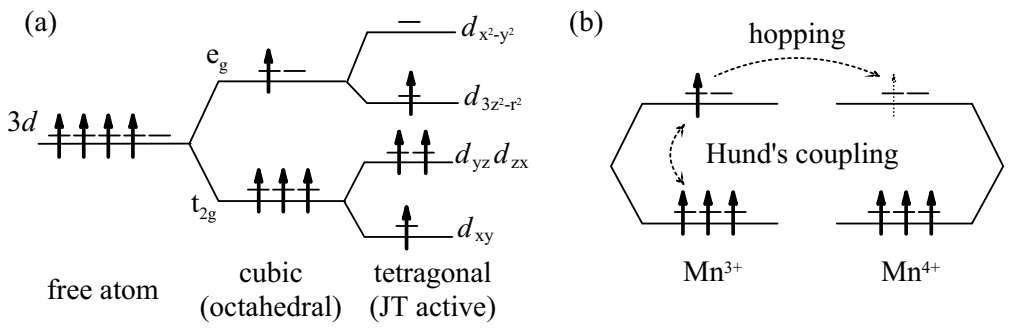

FIG. 2: (a) Cubic and tetragonal crystal field splitting of $3d$ orbitals in Mn^{3+}. (b) A simple representation of ferromagnetic coupling via double exchange.

Fig. 2(a)) Since there is only one electron occupying the e_g level, it occupies the lower energy level leaving the parent compound insulating.[3] As we replace some of the La^{3+} cations with Sr^{2+} cations, we dope carriers into the system in the form of holes on Mn sites. Thus, we will have a mixture of Mn^{3+} and Mn^{4+} ions, and as the carrier concentration is varied, the system's physical properties change as shown in Fig. 3.[4] The ferromagnetic order and metallic conductivity first show up at $x \sim 0.1$ and at $x \sim 0.15$, respectively. When the Sr concentration reaches $x \sim 0.3$, the ferromagnetic transition temperature, T_C, becomes maximum and the material becomes metallic over the entire observed temperature range.

Now, we've suggested how the system becomes metallic at high carrier concentrations, but the question remains, why does it become ferromagnetic (that is, why do the spins on different Mn sites spontaneously align in the same direction?). While there are various causes of magnetism in materials, the dominant factor for the manganites is known as *double exchange*. Here, there is a "virtual process" in which the e_g electrons are allowed to hop from site to site. If you imagine that the e_g electron is hoping from one Mn^{3+} site to a Mn^{4+} site, and back again, it is plausible that the probability of hoping will depend on the relative orientation of spins on the two sites (see Fig. 2(b)). In fact, because of the Hund's rule coupling, as the spin moves from the Mn^{3+} site to the Mn^{4+} site, it would "like" to be aligned with the t_{2g} spins on that site. Thus, if the spins on both sites are aligned, hopping is easier. Thus, ferromagnetism evolves from the system maximizing the probability of hopping. This is the physical basis behind the double-exchange model of Zener.[5]

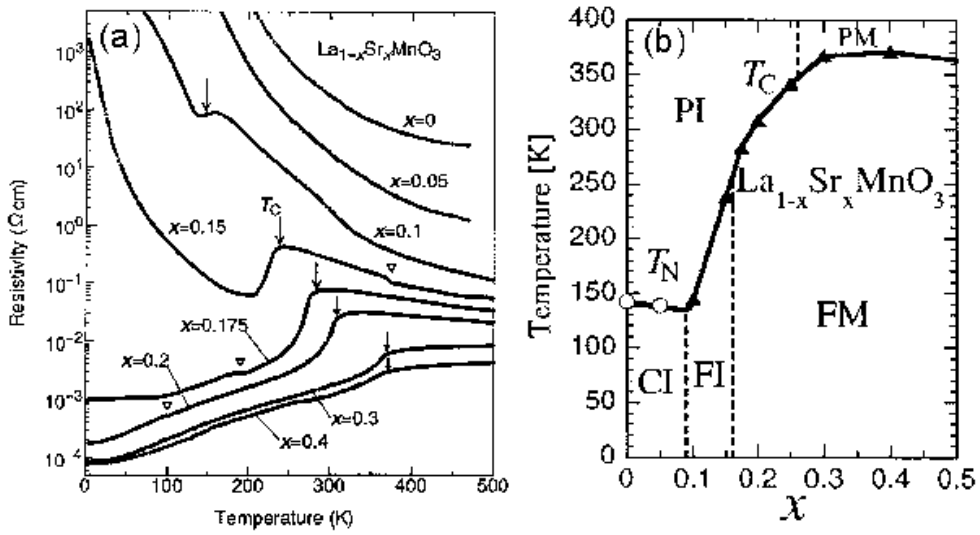

FIG. 3: (a) The resistivity of $La_{1-x}Sr_xMnO_3$ as a function of temperature. The arrows indicate critical temperatures for magnetic transitions. (b) The phase diagram of $La_{1-x}Sr_xMnO_3$ system. For abbreviations, F, P, C, M, and I stand for ferromagnetic, paramagnetic, spin-canted antiferromagnetic, metallic and insulating, respectively.[4]

Question: (1) Based on the picture described above, explain how magnetic field reduces the resistivity in CMR materials. (2) In Fig. 3(b), what would you suggest is the hole doping concentration that is potentially useful for CMR read head application, and why?

II. BASICS OF NEUTRON SCATTERING

A. Neutron as a probe of matter

It is the ability of the neutron to exchange a *measurable* amount of energy with a liquid or solid sample that makes it useful as a probe of the various dynamical phenomena in condensed matter systems.[6] Typical neutron energies available at a reactor source can range from 100 – 500 meV (hot), to 5 – 100 meV (thermal), to 0.1 – 10 meV (cold), where 1 meV = 10^{-3} eV = 8.06 cm^{-1}. A number of different methods can be used to prepare a monochromatic (or monoenergetic) neutron beam having energies that are comparable in

magnitude to, for example, those of the lattice vibrations in a solid (phonons), the spin excitations in a magnetic system (magnons), the torsional, bending, or stretching vibrations of a polymer chain, or the rotational motions in a molecular solid (librons). It is usually quite easy to detect the change in the neutron energy after scattering from a sample since the energy transferred to or from the sample $\Delta E = E_i - E_f$ generally represents a significant fraction of the initial and final neutron energies E_i and E_f.

The energy ΔE transferred during the interaction between neutron and sample can be used to create an excitation (such as a phonon or magnon) of the system, in which case the neutron loses an amount of energy ΔE equal to the energy of the excitation. Conversely, the same excitation can give up its energy to the neutron, in which case the excitation is said to be annihilated. In either case, the physics of the excitation as revealed by the absolute change in the neutron energy is the same. The energy transfer ΔE is often expressed as a frequency of vibration through the relation

$$\Delta E = \hbar\omega, \tag{1}$$

where $2\pi\hbar = h = 6.626 \times 10^{-34}$ Joules-seconds is Planck's constant, and ω is the frequency of vibration of the excitation. Since frequency and time are inversely related, the neutron energy transfer $\hbar\omega$ reflects the *time scale* of the dynamics.

Question: Estimate the value of $(\Delta E/E_i)$ required to observe an optic phonon with an energy of 10 meV using x-ray, light, and neutron scattering techniques assuming the values of E_i = 7,000 eV, 2 eV, and 30 meV (0.030 eV), respectively. Which technique is best suited for this measurement?

In addition to having energies that are well adapted to the study of a large variety of dynamical phenomenon, neutrons also possess the ability to provide, simultaneously, unique information about the *geometry* of these dynamics through the exchange of momentum with the sample. This is done by measuring in what directions (i. e., through what angles) the neutrons scatter. The momentum of a neutron varies inversely with the neutron wavelength λ, and hence an accurate measure of the momentum transferred between sample and neutron during the scattering process will in turn provide information about the spatial scale of the

dynamics being probed. Such an accurate measure is relatively easy to obtain as long as the neutron wavelength is comparable to the length scale of the motions of interest.

Question: The relationship between wavelength and energy for the neutron is given by:

$$E = \frac{h^2}{2m\lambda^2} = 81.81(\text{meV} \cdot \text{Å}^2)/\lambda^2, \tag{2}$$

where $m = 1.675 \times 10^{-24}$ grams is the mass of the neutron. Using this equation, estimate the wavelengths corresponding to hot, thermal, and cold neutrons available at a reactor source. How do these wavelengths compare with the length scales associated with the dynamics or motions you are specifically interested in?

In the following sections we will discuss the partial differential scattering cross section, which is the actual physical quantity that is measured by neutron spectroscopy. We then outline the basic operating principles behind a triple-axis spectrometer (TAS), the concept for which Bertram Brockhouse earned the 1994 Nobel prize in physics shared jointly with Clifford Shull.

B. The Partial Differential Scattering Cross Section $\frac{d^2\sigma}{d\Omega dE_f}$

Most neutron spectroscopic techniques can be reduced to a measurement of what is called the *partial differential scattering cross section*, or $d^2\sigma/d\Omega dE_f$, as a function of the neutron energy transfer $\hbar\omega$ and the neutron momentum transfer $\vec{Q}$.[6] The quantity $\vec{Q}$ is known as the scattering vector, and has units of inverse length. In the scattering process between the neutron and the sample, the total momentum and energy of the system are conserved, i. e.

$$\vec{Q} = \vec{k_i} - \vec{k_f}, \tag{3}$$

$$\hbar\omega = E_i - E_f = \Delta E. \tag{4}$$

Hence the energy or momentum lost (or gained) by the neutron when it scatters from a sample is gained (or lost) by the sample. In the previous equation, the quantities $\vec{k_i}$ and $\vec{k_f}$ refer to the initial and final neutron wavevector, respectively, and point in the direction of

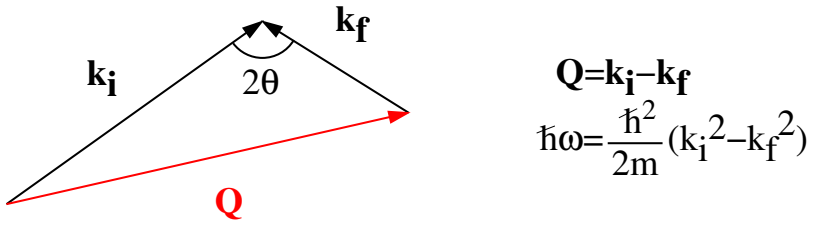

FIG. 4: Scattering triangle. The neutron is scattered through the angle 2θ and the scattering vector, $\vec{Q}$, is given by the vector relationship $\vec{Q} = \vec{k}_i - \vec{k}_f$.

the incident and final (scattered) neutron beam. The relationship between $\vec{k_i}$, $\vec{k_f}$, and $\vec{Q}$ can be represented by the *scattering triangle* shown in Fig. 4. The magnitude of the neutron wavevector k is $2\pi/\lambda$, and is related to the neutron energy via

$$E = \frac{(\hbar k)^2}{2m} = 2.072(\text{meV} \cdot \text{Å})k^2, \tag{5}$$

From this last equation, one can obtain the second equation in Fig. 4 which relates the energy transfer to the magnitude of the initial and final wavevectors. The angle between $\vec{k_i}$ and $\vec{k_f}$ is commonly denoted by 2θ, and represents the total angle through which a neutron is scattered by the sample. Note that the convention followed in this summer school is such that the energy transfer $\hbar\omega$ is positive when $E_i > E_f$, i. e. when the neutron loses energy to the sample during the scattering process. This convention of defining when $\hbar\omega$ is positive varies among neutron scattering facilities.

The partial differential scattering cross section is defined as the total number of neutrons scattered per second by the sample into a unit of solid angle $d\Omega$ in a given direction, having final energies E that lie between E_f and $E_f + dE_f$. It is normalized by the neutron flux incident on the sample Φ_0 (measured in neutrons/sec/cm^2) so that it has units of area/(solid angle)/energy. If one integrates the partial differential scattering cross section over the entire solid angle ($= 4\pi$ steradians), and all final energies ($0 \leq E_f \leq \infty$), one obtains the total number of neutrons scattered out of the beam per second by the sample. (This assumes that the absorption of neutrons by the sample, which can often occur, is negligible.) This is known as the total scattering cross section σ, which has units of area. Thus σ represents the scattering strength of the sample, and can be viewed as an unnormalized probability that an incident neutron will be scattered. If one compares the value of σ for hydrogen with that of aluminum, it will be clear that different elements can have enormously different scattering

strengths.

Question: The scattering cross section for x-rays is a strong and monotonically increasing function of atomic number Z. This is because x-rays scatter from the electrons of an atom, which increases with increasing Z. Neutrons, by contrast, scatter from the atomic nucleus via short-range nuclear forces. If you plot σ for neutrons versus Z, do you see any trend? In what ways might this be advantageous? (Values for σ can be obtained from the NCNR Summer School webpage under "Course Materials," or at http://www.ncnr.nist.gov/resources/n-lengths/.)

It is instructive to consider the relative sizes of σ and $d^2\sigma/d\Omega dE_f$. Clearly σ, which represents the total number of neutrons scattered per second by the sample, is many orders of magnitude larger than $d^2\sigma/d\Omega dE_f$, which is an analyzed quantity both in energy and direction. On the other hand, the partial differential scattering cross section provides a correspondingly greater amount of information because it contains all of the details of the individual and collective motions of the atoms, molecules, and/or any atomic magnetic moments that comprise the sample. The *differential cross section* $d\sigma/d\Omega$, which is what is measured in a diffraction experiment, lies between σ and $d^2\sigma/d\Omega dE_f$ in size. As the elastic component dominates in $d\sigma/d\Omega$, it gives the time-averaged (equilibrium) positions of all of the nuclei in the sample, and is used to determine the crystal structure.

The partial differential scattering cross section can be cast into a useful mathematical form via the formalism outlined at the end of the neutron scattering primer written by Roger Pynn[7] (which the summer student is presumed to have read). With a small deviation from the notation used by Pynn we can write the partial differential cross section for a system composed of a single atomic element as

$$\frac{d^2\sigma}{d\Omega dE_f} = \frac{1}{4\pi}\left(\frac{k_f}{k_i}\right)\left[\sigma_{coh}S_{coh}(\vec{Q},\omega) + \sigma_{inc}S_{inc}(\vec{Q},\omega)\right], \tag{6}$$

where $S(\vec{Q},\omega)$ is exactly same quantity as $I(\vec{Q},\epsilon)$ used by Pynn to express Van Hove's *scattering law*. The subscripts *coh* and *inc* refer to the coherent and incoherent parts of the scattering, and pertain to the collective or individual motions of the atoms, respectively, as described on page 9 of Pynn's primer. For the purposes of this experiment on SPINS,

we are only concerned with the collective dynamics of the magnetic moments present in $La_{0.7}Sr_{0.3}MnO_3$, and thus the coherent part of the partial differential scattering cross section.

The scattering function $S_{coh}(\vec{Q},\omega)$ contains a double sum over pairs of nuclei as shown in Eq. 3 on page 28 of Pynn's primer.[7] Each term in this sum represents the *correlation* between the position of one nucleus at a time $t = 0$ with that of another nucleus at an arbitrary time t later. These correlations are important for systems in which the nuclei are strongly coupled via some type of interaction, and less so when this coupling is weak. In either case $S_{coh}(\vec{Q},\omega)$ provides a measure of the strength of this coupling, and hence the resulting *collective* motions. It is therefore extremely useful, for example, in mapping out the dispersion relations of lattice vibrations, that is how the energy ω of the lattice vibrations changes at different $\vec{Q}$ positions, in solids. For the remainder of this discussion, we will drop the subscript *coh* with the understanding that we are referring to the coherent part of the scattering function.

The scattering function $S(\vec{Q},\omega)$ can be simply related to the imaginary part of the dynamical susceptibility according to

$$S(\vec{Q},\omega) = \frac{\hbar}{\pi}\left(\frac{1}{e^{\hbar\omega/k_BT}-1}+1\right)\chi''(\vec{Q},\omega), \tag{7}$$

where $k_B = 1.381\times10^{-23}$ Joules/K is Boltzmann's constant (note: $\hbar/k_B = 11.60$ K/meV is a handy conversion factor). This is a very important equation since it shows that $S(\vec{Q},\omega)$, which is readily obtained from the experimentally measured partial differential scattering cross section via Eq. (6), is also related to a quantity that is easily calculated by theorists, $\chi''(\vec{Q},\omega)$. The dynamical susceptibility is a measure of how the system responds when it is "wiggled". $\chi''(\vec{Q},\omega)$ refers to the imaginary part of this quantity, which is related to how energy is dissipated by the system. Therefore a measurement of the partial differential scattering cross section via neutron spectroscopy allows for a direct test of theoretical models. By recording the scatterered neutron intensity as a function of energy transfer $\hbar\omega$ and momentum transfer $\vec{Q}$, and removing the instrumental effects, one obtains $S(\vec{Q},\omega)$, which contains all of the dynamical information about the system.

With the exception of the neutron spin-echo (NSE) technique, all other neutron spectroscopic methods measure $d^2\sigma/d\Omega dE_f$ using a neutron detector to count the number of neutrons scattered per unit time from a sample as a function of the energy transfer $\Delta E = \hbar\omega$ and the momentum transfer $\vec{Q}$. To do this requires that one know the energy and wavevector

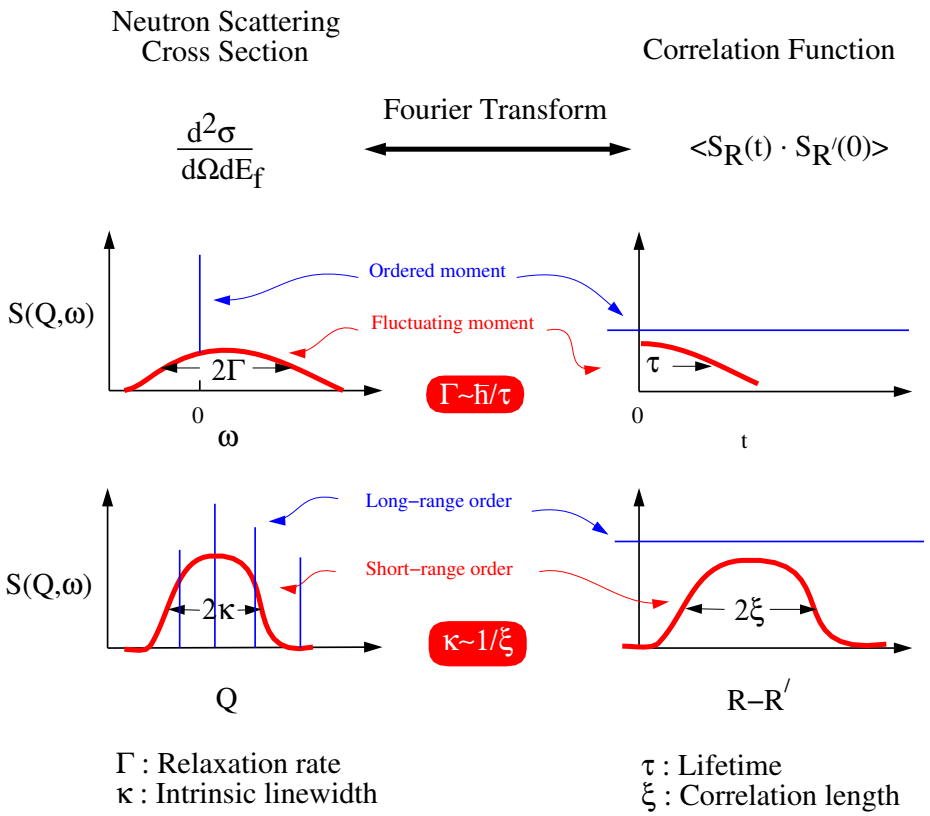

FIG. 5: The relationship between the neutron scattering cross section and the spin-spin correlation function. The relaxation rate Γ is HWHM in energy of $S(Q,\omega)$, and is inversely proportional to the lifetime of the excitation τ. The line-width κ is the HWHM in momentum transfer of $S(Q,\omega)$, and is inversely proportional to the correlation length ξ.

of the neutron before $(E_i, \vec{k_i})$ and after $(E_f, \vec{k_f})$ it scatters from the sample. There are many ways of doing this, and most will be illustrated by the different experiments in this summer school. As will be seen, each method has its own particular advantages and limitations, depending on the range of energy transfers (time scales) and momentum transfers (length scales) one wishes to study.

C. Understanding The Spin-Spin Correlation Function $< S_R(t) \cdot S_{R'}(0) >$

The intensity of neutrons scattered from the magnetic moments in a solid is proportional to the spin-spin correlation function:[6]

$$\frac{d^2\sigma}{d\Omega dE_f} = r_0^2 \frac{k_f}{k_i} |\frac{g}{2} F(Q)|^2 \sum_{\alpha\beta} (\delta_{\alpha\beta} - \hat{Q}_\alpha \hat{Q}_\beta)$$

$$\frac{1}{2\pi\hbar}\int dt\ e^{i\omega t}\frac{1}{N}\sum_{\vec{R}\vec{R}'} < S^{\alpha}_{\vec{R}}(t)S^{\beta}_{\vec{R}'}(0) > e^{-i\vec{Q}\cdot(\vec{R}-\vec{R}')} \tag{8}$$

where $r_0 = -0.54 \cdot 10^{-12}$ cm, g is the gyromagnetic ratio, $F(Q)$ is the magnetic form-factor and N is the number of unit cells in the solid. Basically the partial differential scattering cross section $d^2\sigma/d\Omega dE_f$ is the Fourier transform in space and time of the spin-spin correlation function $< S_R(t) \cdot S_{R'}(0) >$. Thus, neutron elastic scattering probes static ordered moments, whereas neutron inelastic scattering probes fluctuating (dynamic) moments.

While this equation appears formidable, Fig. 5 can help shed substantial light on the relationship between the measured magnetic neutron scattering cross section and the time-dependent spin-spin correlation function. The spatial dependence of the spin correlations can be determined from the Q-dependence of $S(\vec{Q},\omega)$. For example, if $S(\vec{Q},\omega)$ is Q-resolution limited, then this would indicate that the spatial correlations are of long-range. However, if $S(\vec{Q},\omega)$ is broader than the instrumental Q-resolution, then the correlations are short-ranged. A similar argument can be made for linewidths, which is the peak widths observed in energy scans. If $S(\vec{Q},\omega)$ is $\hbar\omega$-resolution limited, then this would indicate that the temporal correlations are of long-range. However, if $S(\vec{Q},\omega)$ is broader than the instrumental $\hbar\omega$-resolution, then the excitations are only short-lived in time.

III. TRIPLE-AXIS SPECTROSCOPY

A. Introduction to The Triple-Axis Spectrometer

The triple-axis spectrometer (TAS) is an extremely versatile instrument that is primarily intended for the study of the collective motions of the atoms and their magnetic moments in single crystal samples. The first TAS system was used to obtain the first experimental demonstration of phonon and magnon dispersion curves (in aluminum and magnetite) in the mid 1950's.[8] The instrument derives its name from the fact that the neutrons interact with three crystals on their way from reactor to detector, each crystal being able to rotate independently about a vertical axis passing through its center. This is shown schematically in Fig. 6. The first crystal is called the monochromator, as it selects a single monochromatic component from the white neutron beam emanating from the reactor or neutron guide. The second crystal is the sample itself (although it may be either a single crystal or a powder). The third crystal is called the analyzer, as it is used to analyze the energy spectrum of the

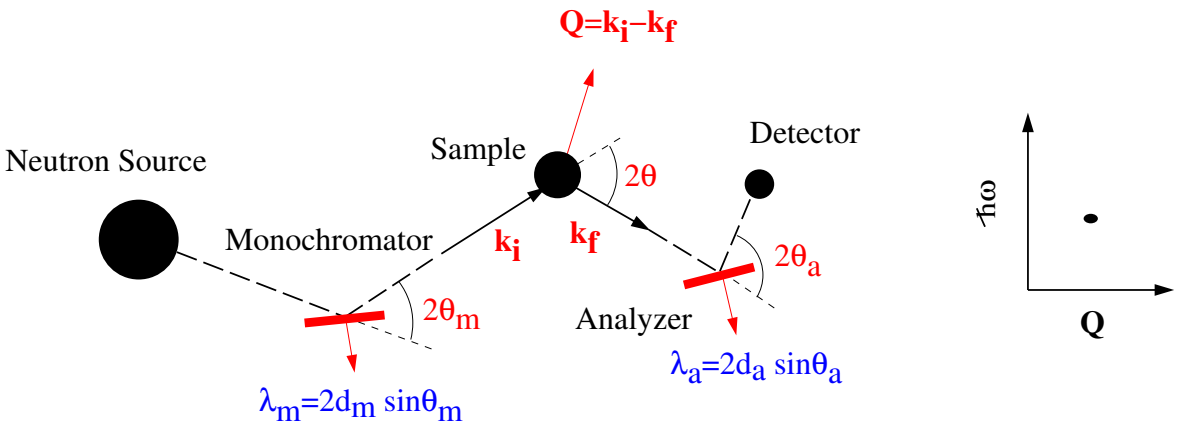

FIG. 6: Schematic scattering configuration for a conventional triple-axis spectrometer. It measures a scattering event at a single value of $(\vec{Q}, \hbar\omega)$ at a time.

neutron beam that scatters from the sample. The last primary element of the instrument is, of course, the neutron detector.

In a triple-axis spectrometer, the initial and final neutron energies are determined by exploiting the process of Bragg diffraction from the monochromator and analyzer single crystals. This is done by rotating the crystals about their respective vertical axes such that a specific set of atomic Bragg planes, having a well-defined interplanar spacing d, makes an angle θ, known as the Bragg angle, with respect to the initial (or scattered) beam direction. When this is done, only neutrons with wavelengths that satisfy the Bragg condition (see pages 9-11 of Pynn's primer)

$$n\lambda = 2d\sin\theta, \tag{9}$$

where n is an integer greater than zero, will Bragg scatter from each crystal and proceed successfully to the next element of the spectrometer.

Question: Because the variable n in Bragg's law can be any integer greater than zero, more than one monochromatic component can be present in the neutron beam diffracted by either monochromator or analyzer. List the possible wavelengths of these other components. How might their presence affect the experimental data?

To remove the extra and unwanted monochromatic components from a Bragg diffracted

beam, while preserving the neutron flux at the desired fundamental (n=1) wavelength λ, it is common practice to place a filter composed of some solid material in the path of the beam. The choice of material depends on the primary wavelength λ. For thermal neutrons, a special form of graphite (pure carbon) known as highly-oriented pyrolytic graphite (HOPG or just PG) is often used. Graphite has a layered structure in which the crystalline [001] or c-axis is normal to the layers. HOPG behaves like a crystal of graphite in which the various graphite layers have all been randomly spun about the c-axis. Therefore HOPG can be viewed as a single-crystal along [001], and a powder along the two orthogonal directions. It exhibits very good transmission at certain neutron energies including 13.7, 14.7, 30.5, and 41 meV. Neutrons of other energies are preferentially (though not completely) scattered out of the beam, thereby minimizing the chance they will enter the detector and contribute to the background.

For cold neutrons, such as those used on the SPINS spectrometer, a polycrystalline block of beryllium (Be) is used as a wavelength filter. The requirement for this filter to work is that there be enough tiny crystallites to span all angular orientations, i. e. all values of the Bragg angle θ, so that all unwanted neutrons are Bragg scattered out of the neutron beam.

Question: (1) Consider a white (polychromatic) beam incident on a polycrystalline Be filter. What happens to those neutrons with wavelengths $\lambda > 2d_{max}$, where $d_{max} = 1.98$ Åis the largest interplanar d spacing available in beryllium? What happens to those neutrons with $\lambda \leq 2d_{max}$? Make a simple sketch of transmission versus energy for this filter.
(2) What are the criteria for ideal materials for designing neutron low-pass filters?

As can be seen from Fig. 6, when the incident neutron beam from the reactor strikes the monochromator, it is scattered through an angle $2\theta_m$ from its initial direction. This is commonly referred to as the monochromator *scattering angle*. In order for the resulting monochromatic beam to hit the sample, it is necessary to rotate the subsequent elements (sample, analyzer, and detector) of the spectrometer about the monochromator axis through an angle of $2\theta_m$. The same situation applies for the sample, and the analyzer, i. e. associated with each crystal is a Bragg angle θ, and a scattering angle 2θ. Hence each axis of the triple-axis spectrometer is actually composed of two motors, one to control the crystal Bragg

angle θ, and the other to rotate the subsequent (downstream) elements of the instrument by the appropriate scattering angle 2θ. While there are many different motors involved in the operation of a triple-axis spectrometer, such as those that control mechanical slits that limit the horizontal and vertical extent of the neutron beam, the primary instrument motors are those that control the values of θ and 2θ for the monochromator, sample, and analyzer. (NOTE: The convention of naming θ and 2θ comes from the fact that $2\theta = 2 \times \theta$ for elastic Bragg scattering. Even though this relation no longer holds for inelastic scattering, they are still called the same way.)

The material most commonly used as monochromator and analyzer in a TAS system is also HOPG. Its utility lies in its very high reflectivity for neutrons over a wide range of energy, along with its negligible incoherent scattering and adsorption cross sections, and its low atomic number so that scattering by gamma rays is small. The (002) Bragg planes of HOPG have an interplanar d spacing of 3.354 Å. Other materials that also find use in triple-axis spectroscopy are silicon, germanium, and copper.

Question: Calculate the monochromator Bragg and scattering angles required to obtain a neutron beam having initial energies $E_i = 14.7$ meV, and 100 meV using the (002) reflection of HOPG. The (220) reflection of copper has a d spacing of 1.278 Å. Would this be a better choice of monochromator in either case?

During the interaction with the sample, neutrons can lose or gain energy, and thus can emerge with an energy $E_f \neq E_i$. The resulting energy transfer can be computed according to

$$\hbar\omega = E_i - E_f = \frac{h^2}{8m}\left(\frac{1}{d_m^2 \sin^2\theta_m} - \frac{1}{d_a^2 \sin^2\theta_a}\right), \tag{10}$$

where d_m and d_a are the d-spacings of the monochromating and analyzing crystals, respectively. If the analyzer is set to select the same energy as that of the incident beam ($E_i = E_f$), then $\hbar\omega = 0$, and the scattering is said to be *elastic*. If not, one detects *inelastic* scattering events. (A third category of scattering known as *quasielastic* scattering, is discussed in the experiment on the Disc Chopper Spectrometer (DCS).)

Measuring the momentum transfer $\vec{Q}$ between neutron and sample is achieved by orienting the incident and final neutron wavevectors with respect to each other to obtain the desired

vector difference $(\vec{k_i} - \vec{k_f})$. Unlike the case of the monochromator and analyzer crystals, the Bragg and scattering angles for the sample needn't be related by a simple factor of 2. Indeed, when measuring inelastic scattering they usually are not. Hence the notation 2θ (which is quite common) can be misleading for the novice scatterer. With this warning in mind, we can calculate the magnitude of the momentum transfer by computing the vector dot product of $\vec{Q}$ with itself, i. e.

$$\vec{Q} \cdot \vec{Q} = (\vec{k_i} - \vec{k_f}) \cdot (\vec{k_i} - \vec{k_f}), \tag{11}$$

from which we obtain

$$Q = \sqrt{k_i^2 + k_f^2 - 2k_i k_f \cos 2\theta}. \tag{12}$$

Note that the momentum transfer does not depend on the sample Bragg angle θ, but only on the sample scattering angle. The purpose of the Bragg angle is to allow the crystalline axes of the sample (if it happens to be a single crystal) to be aligned in specific ways with respect to the scattering vector $\vec{Q}$. This allows one to probe the geometry of the dynamics in question along different symmetry directions. The utility of the sample Bragg angle becomes moot, however, in the case of a powder sample (composed of many tiny and randomly-oriented single crystals).

Question: What is the maximum momentum transfer one can obtain in the case of elastic scattering, i.e. $|\vec{k_i}| = |\vec{k_f}|$? What is the minimum? Why might these two configurations be problematic from an experimental point of view?

By stepping the analyzer Bragg angle θ_a, or the monochromator Bragg angle θ_m, by computer in small angular increments, one can effectively scan the energy transfer $\hbar\omega$. Generally this is done while keeping the momentum transfer $\vec{Q}$ constant, and is known as a constant-$\vec{Q}$ scan. The complement to the constant-$\vec{Q}$ scan is the constant-E scan in which the energy transfer is held constant while one varies the momentum transfer. These two scans are fundamental to the triple-axis method, and are used commonly to map out the dispersion relations for both phonons and magnons in condensed matter systems.

In the case of a constant-$\vec{Q}$ scan, one has the choice of fixing either the incident or final

energy, through fixing the Bragg angles of either the monochromator or the analyzer. As a rule, it is best not to vary both as one needs to place a wavelength filter in the path of either the incident beam (before the sample) or the scattered beam (after the sample) in order to remove the higher order harmonic content of the Bragg diffracted neutron beam (remember the effect of the integer n in Bragg's law). If the analyzer angle θ_a is fixed and one varies θ_m, the result is an E_f-fixed configuration. Doing the opposite results in an E_i-fixed configuration. Both methods yield data that contain the same physics. Deciding which to choose depends largely on the specific problem being studied.

B. Resolution functions in Triple-Axis Spectroscopy

The theoretical scattering function $S_{coh}(\vec{Q}, \omega)$ contains delta functions in momentum and energy, such as $\delta(\vec{Q} - \vec{Q}_o, \omega - \omega_o)$. It means that the scattering intensity will be infinite for $(\vec{Q}, \omega) = (\vec{Q}_o, \omega_o)$ and zero for the rest. However, a measured intensity is always spread out to a finite width in real experiments. One reason could be the short-range correlations in time and space as described in Fig. 5. Even when there is a long-range order, however, one will still observe peaks with non-zero widths. It is because of various experimental uncertainties, such as divergence of the neutron beam or domain misorientations within a sample. Although it may seem like a misfortune, it is in fact a very important element for a practical implementation of the triple-axis spectroscopy, which sometimes is relaxed on purpose. Without finite resolution, one will not only have a difficult time locating desired signals, but also suffer from limited intensity coming from virtually zero acceptance. Below, we briefly discuss the important factors determining experimental resolution of a triple-axis spectrometer.

The monochromator and analyzer crystals are often intentionally processed to introduce small angular misorientations of the Bragg planes. This can be done by pressing the crystals under high pressure and temperature, for example, so the Bragg planes are no longer exactly parallel to each other, but are instead narrowly distributed in angle. Such an angular distribution is often Gaussian in form, and is usually characterized by the full-width at half maximum (FWHM), known as the crystal mosaic. The result is that both monochromator and analyzer will diffract a narrow spread of neutron energies that depends on the size of the mosaic, and significantly increases the scattering intensity measured at the detector. Typical

values for the mosaic spread range from $30'$ (0.5^o) to $40'$. The resulting energy transfers of the neutrons will be distributed about an average value $\hbar\omega_0$.

The introduction of angular misorientation to the monochromator results in not only a spread in neutron energy but also a spread in its direction. Typically a sample mosaic is much larger than the monochromator mosaic, and can be an important factor in determining momentum resolution. To improve or control the divergence, which is often called *collimation*, collimators composed of sets of thin parallel blades are inserted into the beam whose length L and separation v define the limiting divergence η of the neutrons according to

$$\eta = 2\tan^{-1}(v/L) \approx 2v/L. \tag{13}$$

These blades are coated with a strongly neutron absorbing material such as Gd_2O_3 or Cd such that neutrons with a divergence that exceeds η are absorbed and removed from the beam. Typically collimators are inserted in each of the four different flight paths between elements of the spectrometer, i.e. between reactor and monochromator, monochromator and sample, etc. A choice of fine collimation improves the instrumental $\vec{Q}$-resolution at the expense of neutrons counted at the detector. A choice of coarse resolution degrades the $\vec{Q}$-resolution, but increases the neutron count rate. To optimize the experimental data then, it is best to match the $\vec{Q}$-resolution of the instrument with the features of the scattering one is try to measure.

In general, the instrumental $(\vec{Q}, \hbar\omega)$-resolution is a complicated function of the factors discussed above plus $\vec{k_i}$, $\vec{k_f}$, etc.. For a given spectrometer configuration, the instrumental resolution can be expressed as a four-dimensional function of $\hbar\omega$ and $\vec{Q}$ as $R(\vec{Q}-\vec{Q}_0, \omega-\omega_0)$, and is always calculated by computer. The surface of constant probability calculated at $(\vec{Q}, \omega) = (\vec{Q}_0, \omega_0)$, say $R = 50\%$, has a different length in each dimensional axis, so it is often called *resolution ellipsoid*. While one can often extract meaningful results from TAS measurements without needing to take the effects of the finite instrumental resolution into account, all data must be corrected for these effects before they can be compared to theoretical calculations of the scattering function $S(\vec{Q}, \omega)$. Fortunately, the intensity at the detector is well-described by a convolution of the resolution function with the scattering function, i. e.

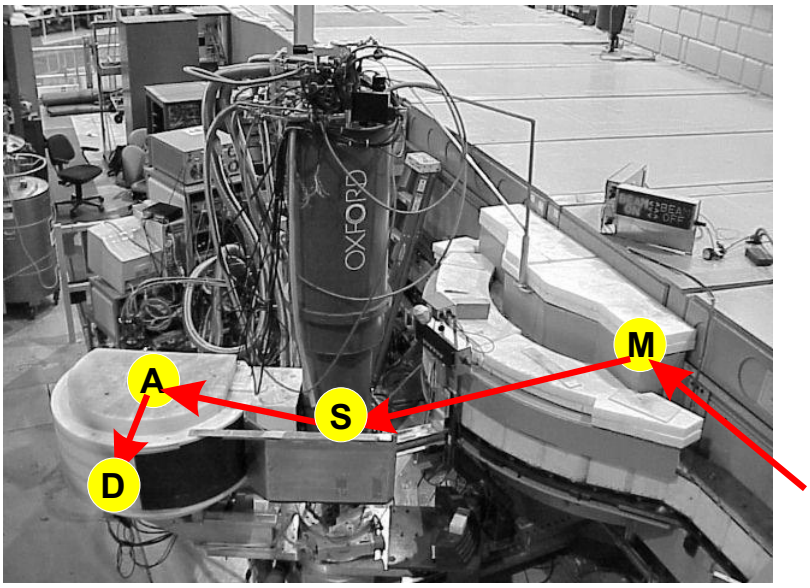

FIG. 7: Overview of the SPINS spectrometer. The arrows show the path of the neutron beam during a scattering experiment. M, S, A, and D stand for monochromator, sample, analyzer, and detector.

$$I_d(\vec{Q}_0, \omega_0) = \int R(\vec{Q} - \vec{Q}_0, \omega - \omega_0) S(\vec{Q}, \omega) d\vec{Q} d\omega. \tag{14}$$

While a detailed discussion of R is beyond the scope of this handout,[9] all users of triple-axis spectrometers will need to know how to optimize the instrumental resolution to match the time scales and length scales of the problem they wish to study.

C. The NCNR Spin Polarized Inelastic Neutron Scattering (SPINS) Spectrometer

The SPINS spectrometer is a cold-neutron triple-axis spectrometer. Fig. 7 show an overview of the SPINS spectrometer and the schematics of the neutron path. It was designed to be operated in various configurations including (1) conventional triple-axis mode, (2) horizontally focusing mode, and (3) multiplexing mode. Polarized-neutron scattering mode is also optionally available. Since the conventional triple-axis mode has been discussed previously (see Fig. 6), below we describe the other two modes of operation. Since many components of the SPINS instrument can be changed as necessary, other modes not described here are also possible.

(a) Horizontally focusing mode: The analyzer of the SPINS spectrometer consists of 11

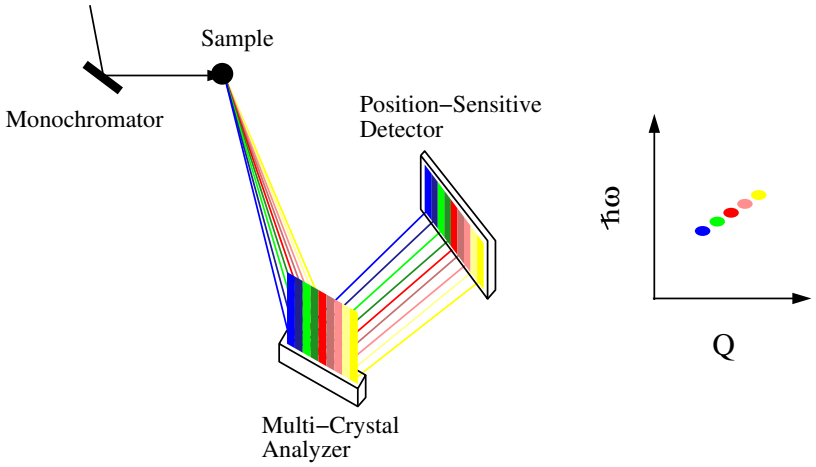

FIG. 8: Schematic scattering configuration of a multiplexing detection system utilizing a Position-Sensitive-Dector (PSD) for a triple-axis spectrometer. It simultaneously measures scattering events at different values of $(\vec{Q}, \hbar\omega)$.

blades of PG crystals that are standing vertically in a row. Each blade is motorized, so it can be individually rotated. If all of the blades are flat with respect to each other, only one of the blades will satisfy the exact Bragg condition, and the scattered beam from other blades will not reach the detector. On the other hand, one can individually align blades so that the scattered beams are focused into the single detector. It has an effect of relaxing momentum resolution but at the same time the detected intensity is increased roughly proportionally to the number of focused blades. Ideally the blades need to be positioned on an arc of a circle encompassing the positions of the sample and the detector. In practise, one can achieve an approximate focusing condition by placing the row of the blades tangential to the relevant arc. This mode of operation is quite useful when studied features are broad in momentum space.

(b) Multiplexing mode: We have discussed before that, if all of the blades are fixed flat, the scattered neutrons will not reach a single detector position. It suggests that one can recover all of the scattered neutrons by utilizing a wide area detector instead. By the combination of 11 flat analyzer blades and an area detector which has a sensitivity in its areal positions, the momentum information from individual blades can be discriminated. What is important in this case is that each blade will produce information not only with different momentum transfer but also different energy transfer. The diagram of the multiplexing mode is shown schematically in Fig. 8.

IV. EXPERIMENT AND ANALYSIS

A. Simple ferromagnetic spin-waves

Perhaps one of the simplest microscopic models of magnetism starts from the Heisenberg Hamiltonian and is generally applicable to insulators (or more formally, systems in which the spins are localized), in which the spin interactions are mediated between overlaps of the atomic wave-functions of electrons living on magnetic ions directly, or through intermediaries such as oxygen. The resulting magnetism originates from a combination of the Coulomb repulsion and the Pauli exclusion principle. In this model, the interaction energy between two neighboring spins is simply:

$$E = -J\mathbf{S}_1 \cdot \mathbf{S}_2 \tag{15}$$

where J is the *exchange constant* representing the strength of magnetic exchange, and $\mathbf{S}_i$ is a vector operator of the ith spin. If J is positive, then a lower energy occurs when the moments are parallel and the ground state at zero temperature will be a ferromagnet as in the present case of interest. If J is negative, then the nearest-neighbor spins will align antiparallel to lower their energies, and this is called an antiferromagnet. (See Fig. 9(a))

But given the ground state of the system, what of its excitations? One of the simplest excitations we could imagine is to simply flip the direction of one of the spins. However, the energy cost of this would be large ($12J$ for a cubic lattice). A much lower energy excitation can be achieved if this spin reversal is shared among many spins. Classically, if we allow the spins to precess about their axes, then a spin-wave can be thought of as a constant phase difference between the precession rates of neighboring spins. (See Fig. 9(b))

The measured spin wave dispersion relation at low temperatures for $La_{.85}Sr_{.15}MnO_3$, which is similar to the sample we are going to study, is shown in Fig. 10. We can see that the energy of the spin waves at small q (long wavelength) is quite small, while at the zone boundary, the excitation energy rises to a relatively high energy of 55 meV (short wavelength excitations mean that the excitation is shared by fewer spins and that neighboring spins are out of alignment to a greater extent, thus requiring more energy to excite). Cold neutron spectroscopy is best applicable to low energy excitations ($\lesssim 10$ meV), and consequently we will be investigating the spin wave excitations at small q in this experiment. The solutions

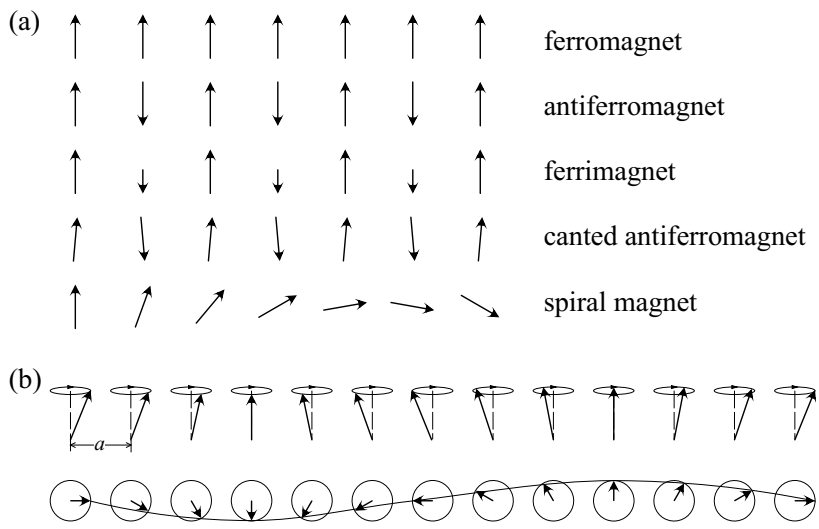

FIG. 9: (a) Examples of simple magnetic ordering patterns. (b) Classical representation of spin wave excitation in an one-dimensional ferromagnet.

to the equations of motion for our simple hamiltonian gives the following dispersion relation:

$$E = 8SJ\sin^2(\frac{qa}{2}) \tag{16}$$

For small q, we may expand the sine function in the dispersion relation to obtain the approximate expression $E \approx 2JSa^2q^2$. We should also include the possibility of magnetic anisotropy in the system. In real spin systems, the moments prefer to point along one particular crystallographic direction and this is represented by the gap parameter, Δ. This particular direction is called the magnetic easy axis, and Δ represents the energy required to rotate the spins away from this easy direction. A "soft" ferromagnet is one where Δ is small, as we are expecting for the present system. For a "hard" or "permanent" magnet, such as on your refrigerator, this costs a lot of energy, and Δ will be large.

In general, the spin wave spectrum changes with temperature. As we increase the temperature, we can thermally excite spin waves and these spin waves gradually destroy the ordered state. There are also collisions between spin-waves. Generally, we can write the spin wave dispersion relation in the small q regime as:

$$E_{SW} = \Delta + D(T)q^2 + E(T)q^4 + ... \tag{17}$$

where D is the spin-wave "stiffness", and the rest of the terms are higher order terms in a

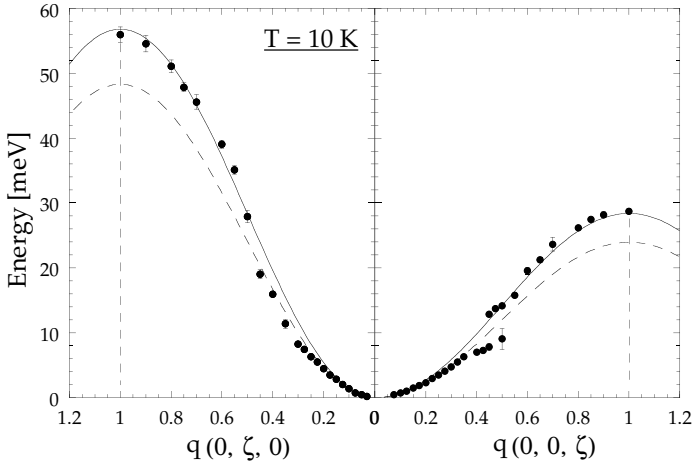

FIG. 10: Spin wave dispersion in $La_{0.85}Sr_{0.15}MnO_3$. The wave vectors are based on the orthorhombic representation.[10]

Taylor expansion. The quantitative value of the stiffness constant D depends on the details of the interactions and the nature of the magnetism, such as whether the magnetic electrons are localized or itinerant, or the structure is amorphous or crystalline, but the general from of the spin wave dispersion relation is the same for all isotropic ferromagnets. As $T \longrightarrow T_C$, in the critical regime just below magnetic ordering temperature T_C, $D(T)$ should follow a power law given by

$$D(T) \propto (1 - \frac{T}{T_C})^{\nu' - \beta} \tag{18}$$

where ν' ($\sim \frac{2}{3}$) is the critical exponent for the correlation length below T_C and β is the critical exponent for the temperature dependence of the magnetization. At elevated temperatures, there will also be many spin waves in the system, and collisions between the spin waves will result in decays of normal modes and consequently finite intrinsic lifetime. The intrinsic line-widths of the spin wave excitations in the long wavelength regime are expected to follow:

$$\Gamma(q, T) \propto q^4 (T \ln \frac{kT}{E_{SW}})^2 \tag{19}$$

Finally, we can determine the number of spin waves that are thermally populated at each temperature and energy, which is directly related to the intensity of the spin waves. These are boson (bosons are particles in which there are no restrictions on the number of particles existing in the same state.) excitations, and should obey the Bose-Einstein population factor:

$$n(E) = \frac{1}{e^{\frac{E_{SW}}{kT}} - 1} \tag{20}$$

Neutrons can annihilate a spin wave excitation in the sample, and gain energy; the probability for this process to occur is directly proportional to the number of spin waves $n(E)$ at the spin wave energy E_{SW}. The neutrons can also create a spin wave in the system, while losing energy. The probability for this process is proportional to $1+n(E)$, where the 1 comes from the fact that is always possible to create a spin wave excitation, even at $T = 0$. This is something that we should also be able to extract from the experimental data.

B. Experimental Planning and Setup

When planning neutron scattering experiments, it is important to have as much understanding as possible of the basic properties of the material. For instance, understanding of the crystallographic information, such as lattice parameters, is imperative. In the case of single crystal samples, it is also important to have some idea about the direction of principal crystal axes. For an effective investigation, measurements of bulk properties such as the magnetic susceptibility, heat capacity and resistivity, can serve as an invaluable guide. All NCNR facility users should avail themselves of any existing data, be it their own, or published elsewhere, that could help them make more efficient use of their beam time.

Crystallographically, $La_{0.7}Sr_{0.3}MnO_3$ belongs to a space group $R\bar{3}c$ with the lattice parameters $a = b = 5.5084$ Å, $c = 13.3717$ Å, $\alpha = \beta = 90^o$, and $\gamma = 120^o$. This hexagonal geometry is equivalent to a rhombohedral one with $a = b = c = 3.8835$ Å and $\alpha = \beta = \gamma = 90.344^o$. Since it is close enough to cubic symmetry, we will do the measurement based on the cubic notation for convenience. Fig. 3(b) shows the ferromagnetic transition temperatures, T_C, of $La_{1-x}Sr_xMnO_3$ as a function of x. $La_{0.7}Sr_{0.3}MnO_3$ has $T_C \sim 350$ K. Therefore, we need sample environment equipment that can control higher than room temperature in order to study the ferromagnetic transition.

Question: (1) $La_{0.7}Sr_{0.3}MnO_3$ orders ferromagnetically below $T_C = 350$ K. Where in the reciprocal space do we have to search for the spin wave excitations?
(2) How would the fluctuations be different between above and below T_C?

The primary goal of this experiment is to measure spin excitation spectrum from the ferromagnetically ordered phase and understand its temperature-dependent behavior. A $\sim$ 4 gram single crystal sample of $La_{0.7}Sr_{0.3}MnO_3$ has been sealed inside an aluminum container. Aluminum is among the most commonly used materials for sample containers because it is relatively transparent to neutrons. The container has been mounted inside a He closed-cycle refrigerator/furnace that can be controlled between 30 - 600 K, and placed on top of the SPINS goniometer (or sample) table. The measurement will be done in the temperature range between 30 and 400 K.

The incident neutron energy on SPINS can be varied from $2.4 \leq E_i \leq 14$ meV. A 6-inch, liquid-nitrogen cooled, polycrystalline BeO filter, which transmits only neutrons having energies below the Bragg cutoff energy of 3.7 meV, Bragg scatters all other neutrons out of the transmitted beam. It has been placed after the sample to eliminate higher-order ($n > 1$) monochromatic components passed by the monochromator. The energy of the analyzer blades has been set to 3.6 meV, so the allowed range of energy transfer is $-1.2 \leq \Delta E \leq 10.4$ meV.

Question: Why is the SPINS BeO filter cooled?

Our measurements will proceed as following. (Some data sets may be taken in advance and distributed.) (1) First, we will measure the integrated intensity of (1 0 0) peak as a function of temperature in the range 250 – 400 K. To properly obtain integrated intensities, one needs to perform both transverse (θ) and longitudinal ($\theta - 2\theta$) scans. From this, we will be able to extract T_C of the sample. (2) Second, we will measure the spin wave spectrum up to $\Delta E \sim 10$ meV by scanning incident energy at several Q points. From the measured data we can obtain the spin wave dispersion, which can be fitted to extract the spin wave stiffness constant, D. The spin wave data may be taken at a few selected temperatures, and the collection of data can be used to show how D changes as a function of temperature. (3) Third, we will measure the quasielastic intensity at a certain $\mathbf{Q}$ close to (1 0 0) over a temperature range going through T_C. The measurement will also be done by scanning incident energy. By analyzing the integrated intensities and the line-widths of the quasielastic peaks as functions of temperature, we will be able to gain insights to the spin dynamics in the vicinity of the

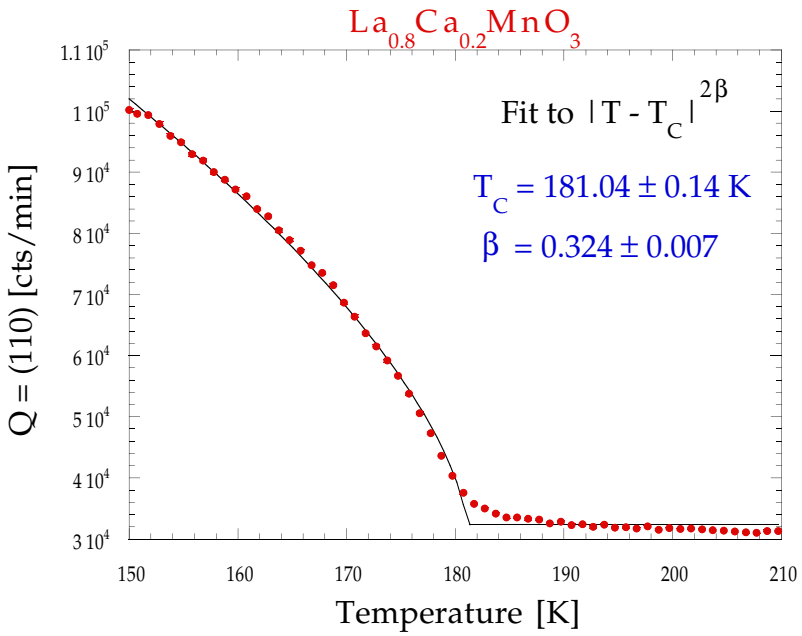

FIG. 11: Temperature dependence of the integrated intensity of the ferromagnetic (1 0 0) peak in $La_{0.8}Ca_{0.2}MnO_3$.[11]

transition.

Question: (1) A θ scan may show multiple peaks instead of a single Gaussian. What could be the reason if it does??
(2) Although it is not the case for the (1 0 0) peak in $La_{0.7}Sr_{0.3}MnO_3$, what would it mean if a $\theta - 2\theta$ scan shows multiple peaks?

C. Data and analysis

Fig. 11 shows the temperature dependence of the integrated intensity of (1 0 0) Bragg peak observed from $La_{0.8}Ca_{0.2}MnO_3$. There is an intensity increase observed around $T_C = 181\ K$ following a power law behavior. This intensity increase comes from ferromagnetic order on Mn sites. The sample we are going to study, $La_{0.7}Sr_{0.3}MnO_3$, will show T_C at a different temperature, but the data will look essentially similar. Knowing that spin waves are fluctuations of ordered spins around average moment, one should expect to observe spin excitation spectrum in the vicinity of this reflection. The (1 0 0) position is particularly

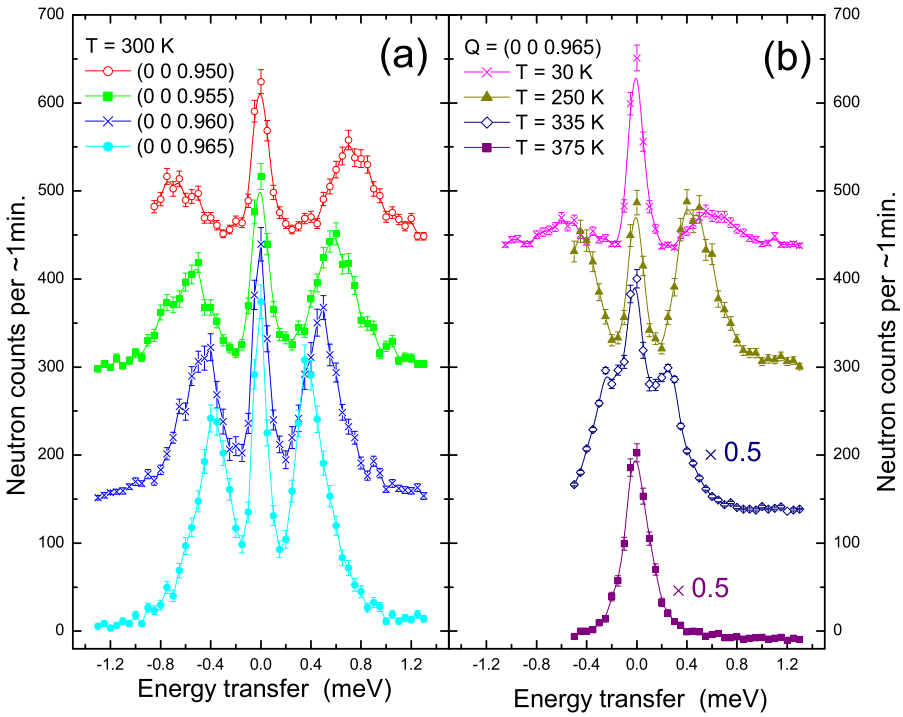

FIG. 12: Constant-Q scans revealing spin wave excitations for $La_{0.7}Sr_{0.3}MnO_3$ (a) at T = 300 K and (b) **Q** = (0 0 0.965).

advantageous, since it is the smallest wave vector where ferromagnetic intensity is observed. It is because magnetic scattering intensity generally decreases at higher momentum transfer due to spatial distribution of unpaired electron density around nuclei.

Question: Why does the ferromagnetic peak position coincide with nuclear peak, say, at (1 0 0)? How about antiferromagnets?

The energy scan data we are going to obtain will be similar to what is shown in Fig. 12. Constant-Q scans typically show three peaks: a central (quasi)elastic peak and an inelastic spin wave peak on each side of positive and negative energy transfer. Fig. 12(a) shows that the spin wave energy increases as we move away from the ferromagnetic (0 0 1) peak. The temperature dependence of D is suggested in the data shown in Fig. 12(b). Although the lineshape of triple-axis data is a complex function of various parameters,

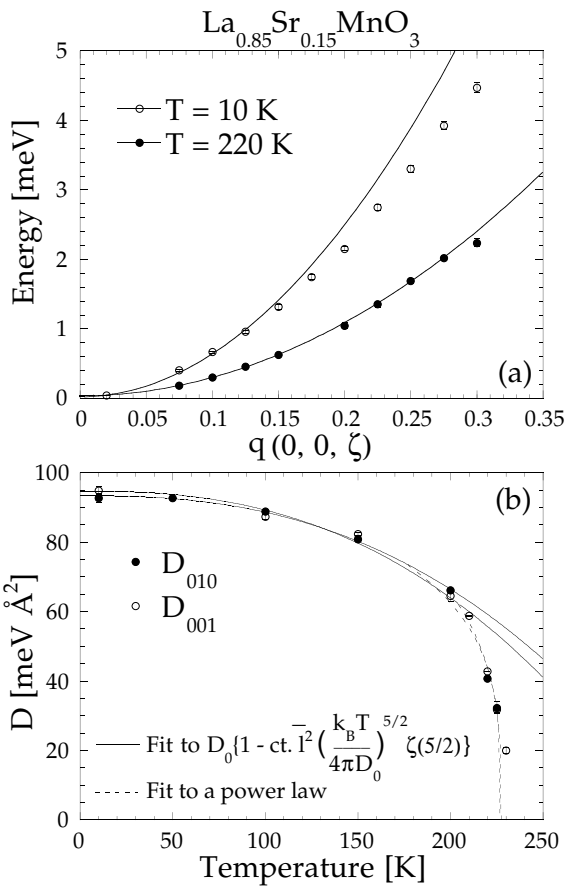

FIG. 13: (a) Low energy spin wave dispersions and (b) the temperature dependence of the spin wave stiffness constant of $La_{0.85}Sr_{0.15}MnO_3$.[10]

one can approximately extract the energy values by fitting with Lorentzian functions. A series of energy values obtained at various momentum transfer can be used to obtain the dispersion relation. The dispersion relation in an isotropic ferromagnet can be conveniently expressed by Equation (17), where the temperature dependent spin stiffness constant was denoted as $D(T)$. Fig. 13(a) shows results obtained from $La_{0.85}Sr_{0.15}MnO_3$ at two different temperatures, and the obtained $D(T)$ are plotted in Fig. 13(b). The quantitative value of the stiffness constant D depends on the details of the interactions and the nature of the magnetism, but the general form of the spin wave dispersion relation is the same for all Heisenberg ferromagnets.

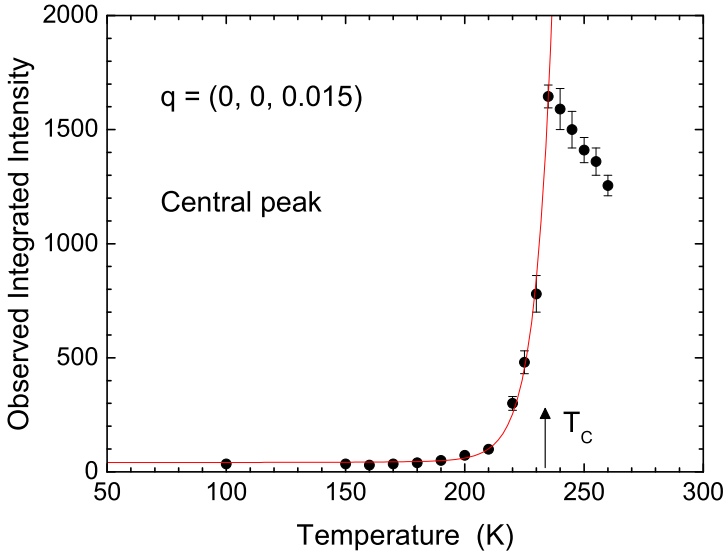

FIG. 14: Integrated intensity of the quasielastic peaks of $La_{0.85}Sr_{0.15}MnO_3$ at (0 0 1.15) as a function of temperature.[10]

Question: (1) What could be the reason that D changes with temperature? What does it mean physically that $D \longrightarrow 0$ for $T \longrightarrow T_C$?
(2) Why is the peak intensity always higher at $\Delta E > 0$ than at $\Delta E < 0$? How would it change with temperature?

Finally, the integrated intensities of the quasi-elastic central peaks are obtained and the result will be similar to what is shown in Fig. 14. These data were obtained slightly away from the zone center, since otherwise the counts will be swamped by the intense nuclear Bragg scattering. The central peak slowly gained intensity approaching T_C in the paramagnetic phase, which quickly dropped below T_C. The intensity above T_C mostly comes from paramagentic fluctuations, while that below T_C is mostly nuclear incoherent background. It shows that we can observe the spectrum from spin dynamics even when there is no long-range magnetic order. What is not shown in the plot is the linewidths as a function of temperature. These data, if available, will give us an idea of the time scale associated with the magnetic fluctuations.

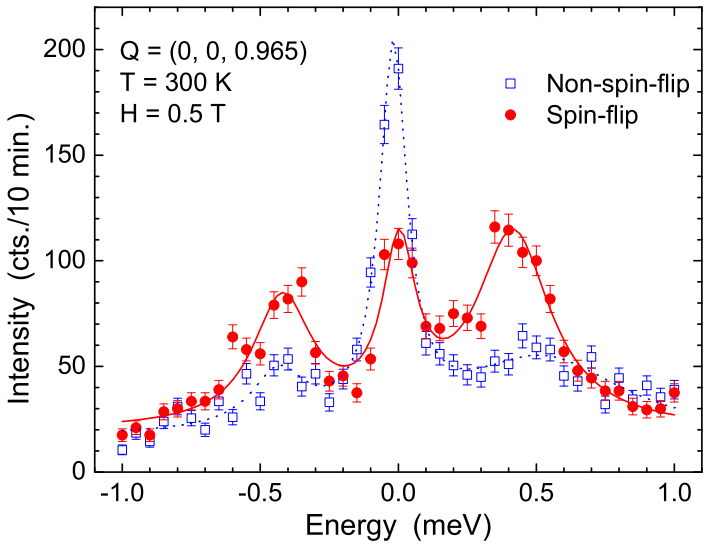

FIG. 15: An energy scan through spin wave excitations in $La_{0.7}Sr_{0.3}MnO_3$ with spin-flip and non-spin-flip channels. The difference in intensity clearly shows that the inelastic signal is due to magnetic scattering while the elastic central peak is mostly nuclear. (Courtesy of Jeff Lynn)

Question: (1) What will Fig. 14 look like if we have measured at several different Q points? Do you expect that the paramagnetic fluctuations will have Q-dependence? If they do, or don't, what would it mean?
(2) What does the change of linewidths in the quasielastic peak suggest? The hint is given in Fig. 5.

D. Polarized Neutron Scattering

We have previously learned that neutrons interact either with nuclei or with unpaired electrons. While it is useful to have more than one type of neutron-sample interaction, it can also be a source of confusion. Therefore, it becomes an important issue how to discriminate magnetic scattering from nuclear scattering. There are several experimental methods to do this, such as probing Q-dependence or temperature-dependence of intensity. Above all, the most powerful and unambiguous method is the neutron polarization analysis. (See Primer p. 24 – 26) It takes advantage of the fact that a neutron can spin flip for magnetic

scattering while it can not for coherent nuclear scattering. Since the neutron polarization analysis involves many experimental complications, such as additional equipment, reduced intensity and a necessity for multiple measurements, we will not perform this during the summer school. Nevertheless, data shown in Fig. 15, which were previously taken with this technique, powerfully confirm that the excitations we observe in $La_{0.7}Sr_{0.3}MnO_3$ are truly magnetic in nature.

---

[1] M. Imada, A. Fujimori, and Y. Tokura, Rev. Mod. Phys. **70**, 1039 (1998).

[2] H. A. Jahn and E. Teller, Proc. R. Soc. London A **161**, 220 (1937).

[3] A.J. Millis, P.B. Littlewood, and B.I. Shraiman, Phys. Rev. Lett, **74**, 5144 (1995). This is a short article titled, "Double Exchange is not enough" which describes the short comings of the double exchange model to Manganites

[4] A. Urushibara, Y. Moritomo, T. Arima, A. Asamitsu, G. Kido, and Y. Tokura, Phys. Rev. B **51**, 14103 (1995).

[5] Zener, C., Phys. Rev. **82**, 403 (1951).

[6] S.W. Lovesy, *Theory of Neutron Scattering from Condensed Matter*, Oxford, (1984).

[7] R. Pynn, *Neutron Scattering - A Primer*, Los Alamos Science Summer (1990).

[8] B.N. Brockhouse, Rev. Mod. Phys. **67**, 735751 (1995).

[9] G. Shirane, S.M. Shapiro, and J.M. Tranquada, Appendix in *Neutron scattering with a triple-axis spectrometer : basic techniques*, Cambridge University Press (2002).

[10] L. Vasiliu-Doloc, J.W. Lynn, A.H. Moudden, A.M. de Leon-Guevara, and A. Revcolevschi, Phys. Rev. B **58**, 14913 (1998).

[11] C.P. Adams, J.W. Lynn, V.N. Smolyaninova, A. Biswas, R.L. Greene, W. Ratcliff II, S-W. Cheong, Y.M. Mukovskii, and D.A. Shulyatev, Phys. Rev. B **70** 134414 (2004).

[12] For a review of the experimental technique and measurements in amorphous ferromagnets see J.W. Lynn and J.A. Fernandez-Baca, Chapter 5 in *The Magnetism of Amorphous Metals and Alloys*, ed. by J.A. Fernandez-Baca and W-Y. Ching (World Scientific, New Jersey (1995), p. 221; J.W. Lynn and J.J. Rhyne, "Spin Dynameics of Amorphous Magnets", in *Spin Waves and Magnetic Excitations*, Part II Chapter 4, p 177, A.S. Borovik-Romanov and S.K. Sinha, editors (North Holland 1988).

V. APPENDIX

A. A Short Note on The Calculation of Spin Wave Dispersion

In order to calculate spin wave dispersions, one needs a good understanding, or at least have a reasonable model, of a spin Hamiltonian describing magnetic energy of the system. Typically it will include the crystallographic coordinates, spin orientations, exchange constants, and/or anisotropy constants, etc.. The simplest spin Hamiltonian is the isotropic Heisenberg model given by:

$$\mathcal{H} = -\sum_{i,j} J_{ij}\ \mathbf{S}_i \cdot \mathbf{S}_j \tag{21}$$

where the $\mathbf{S}_i$ is spin S operator on ith site and J_{ij} is the Heisenberg exchange constant between spins on the ith and jth sites. The quantum fluctuation of a spin away from its classical direction $\tilde{z}$ is expressed by the annihilation and creation operators, $a_i^\dagger$ and a_i, following Holstein-Primakoff formalism:

$$\begin{aligned} S_i^{\tilde{x}} &= \sqrt{\frac{S}{2}}(a_i^\dagger + a_i) \\ S_i^{\tilde{y}} &= i\sqrt{\frac{S}{2}}(a_i^\dagger - a_i) \\ S_i^{\tilde{z}} &= S - a_i^\dagger a_i, \end{aligned} \tag{22}$$

which is derived from a linear approximation satisfying the spin commutation relation. They can be transformed to a global coordinate by

$$\begin{pmatrix} S_i^x \\ S_i^y \\ S_i^z \end{pmatrix} = \mathbf{R}_i \begin{pmatrix} S_i^{\tilde{x}} \\ S_i^{\tilde{y}} \\ S_i^{\tilde{z}} \end{pmatrix} \tag{23}$$

where, $\mathbf{R}_i$ is a rotational matrix corresponding to the relative rotation between the global z axis and the local $\tilde{z}$ axis. After inserting the spin operator of each sublattice into the Hamiltonian and applying Fourier transformation, only the zeroth and the quadratic terms in the creation/annihilation operators are considered. Finally, the Hamiltonian can be diagonalized by Bogoliubov transformation to obtain one magnon dispersion relations. A detailed description of the calculation is beyond the scope of this Summer School.

For commensurate order, where the magnetic lattice is an integer-multiple of the crystallographic lattice, the number of modes is equal to the number of magnetic sublattices.

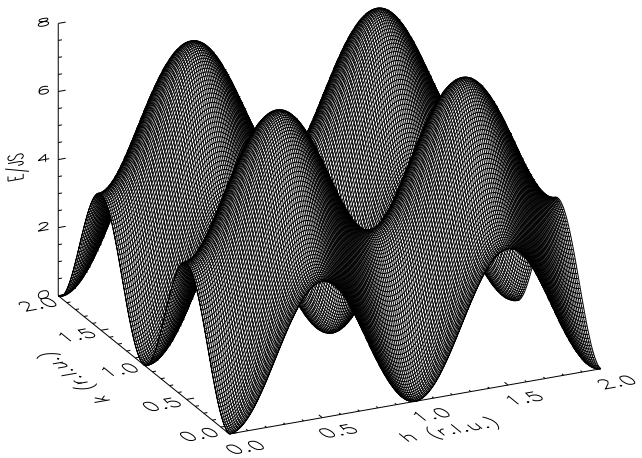

FIG. 16: The surface plot of the spin wave dispersion relations for an isotropic ferromagnet on the (h k 0) plane.

A ferromagnetic simple cubic lattice, similar to $La_{0.7}Sr_{0.3}MnO_3$, has only one sublattice, therefore one normal mode. For the case where nearest neighbor exchange is dominant, the dispersion relation is given as following:

$$\hbar\omega = 4JS\{3 - cos(2\pi h) - cos(2\pi k) - cos(2\pi l)\} \tag{24}$$

The above equation suggests that the dispersion is isotropic near the zone center regardless of the direction of q, which is typical of isotropic Heisenberg ferromagnets. The inclusion of next nearest neighbor exchanges will modify the term J in the equation, but will not affect the isotropy.

Question: Explain how the above dispersion relation agrees with the quadratic dependence on q for an isotropic ferromagnet at small q limit, for instance, shown in Eq. (17).